Electrostatic impacts of plasmonic structure on the performance of monolithically integrated hybrid III-V/Si waveguide-coupled photodetectors

Q. DING,[1,*] 🆔 S. SANT,[2] AND A. SCHENK[1]

[1]*Department of Information Technology and Electrical Engineering, Gloriastrasse 35, ETH Zurich, Zurich, 8092, Switzerland*
[2]*now at Infineon Technologies AG, Neubiberg, 85579, Germany*
[*]*dingq@iis.ee.ethz.ch*

Abstract: 3D opto-electrical simulations are employed to investigate impacts of a plasmonic structure on the performance of a hybrid III-V/Si waveguide-coupled p-i-n $In_{0.53}Ga_{0.47}As$ photodetector with butt-coupling scheme. The plasmonic device is formed by placing an Ag strip on the i-region. The resultant frequency response curves show a strong dependency on the Schottky barrier height at the metal/i-region interface. Quantum efficiency and 3dB bandwidth are generally degraded, except when the barrier is higher than 0.4 eV. The observed effects are mainly due to electrostatic changes in the i-region induced by the Schottky interface.

1. Introduction

The design of high-performance waveguide-coupled photodetectors (WGPDs) suitable for monolithic integration is an essential step in the development of future ultra-fast Terahertz (100 GHz to 10 THz [1]) on-chip communication systems. Performance features required for such application include high detection speed, high responsivity, and small footprint [2]. Conventional WGPDs utilizing dielectric modes usually have dimensions on the μm-scale due to the diffraction limit, and thus hardly fulfill these requirements. Plasmonics has emerged as a promising solution to this problem because of its ability to confine light into small volumes by coupling photons in dielectric materials with the motion of electrons in metals. The formed surface-plasmon polaritons (SPPs) at the dielectric/metal interface have a much smaller wavelength compared with that of the original photons, enabling sub-wavelength scale confinement. Therefore, plasmonic photodetectors could in principle operate at higher speed, as carrier transit time and junction capacitance can be reduced with decreased device dimensions. Such plasmonic enhancement has been recently demonstrated in Schottky-type photodetectors with MSM [3] or metal stripe embedded [4,5] configuration. However, to the best of our knowledge, a similar study has not yet been reported for waveguide-integrated III-V p-i-n photodetectors, which is probably one of the most promising device types for CMOS-compatible monolithic integration. It is, therefore, still an open question whether plasmonics could also be beneficial for this type of device.

The main purpose of this work is to clarify the above issue. To do so, we performed 3D opto-electrical simulations to investigate the impacts of a plasmonic structure on the performance of hybrid III-V/Si co-planar p-i-n type WGPDs. The study is based on our former designed butt-coupled device with n-offshoots [6] where plasmonics is introduced by placing an Ag strip on top of the i-region. Details of the device structure are described in section 2.. The device performance is characterized by quantum efficiency (QE) and 3dB bandwidth as commonly used for photodetectors, which can be extracted from the simulated frequency response curves. The effect of a plasmonic structure on the performance is quantified by the comparison with the original devices without metal strip. Varying the Schottky barrier height (SBH) from 0.1 eV to

0.6 eV in the plasmonic devices reveals that it strongly affects the shape of the frequency response curve. It turns out that the performance change induced by the plasmonic structure is mainly due to the alerted electrostatics in the i-region covered by the metal. Specifically, the electric field is modified in the presence of a Schottky interface, both in terms of spatial distribution of its intensity and direction, depending on the barrier height.

2. Design of device structure

The originally designed non-plasmonic butt-coupled device consists of an $In_{0.53}Ga_{0.47}As$ p-i-n photodetector and a Si waveguide that is horizontally coupled to it [see Fig. 1(a)]. The n-regions are moved aside (thus called as "n-offshoots") in the studied device to avoid an undesired degradation of the QE due to light absorption by metal contacts on this region, which has been shown in our former study [6]. The co-planar integration of III-V materials with Si is feasible for fabrication thanks to the TASE technology developed by IBM-Research Zurich [7]. A detailed description of the fabrication process of a similar butt-coupled p-i-n diode was reported in [8].
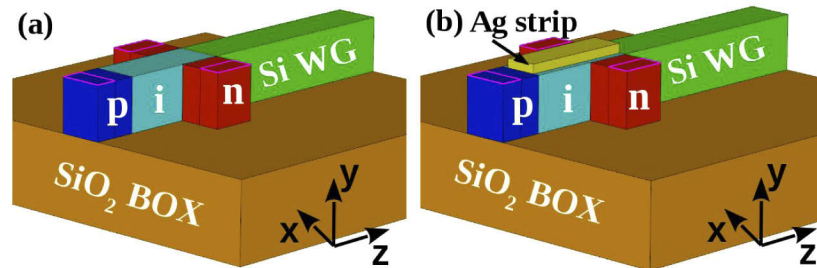
Fig. 1. Sketch of non-plasmonic (a) butt- and (b) side coupled hybrid III-V/Si WGPD. Insertions show corresponding plasmonic devices with an Ag strip on i-region.

The optimized geometrical parameters for non-plasmonic devices in our former work are directly used in this study, including the i-region length in light propagation direction of 500 nm and the Si waveguide height of 240 nm. The waveguide length in light propagation direction is assumed to be 1 μm. All the other dimensions, such as waveguide width and p/n-contact region length in carrier transport direction, are set to 200 nm, following fabrication requirements. The plasmonic device is formed by placing an Ag strip on top of the i-region, as illustrated in Fig. 1(b). The metal strip is set to be 500 nm long, 140 nm wide and 40 nm thick in the corresponding plasmonic device, placed symmetrically with respect to the central line of the i-region.

3. Simulation results and discussion

First, details of the employed simulation methodology, initial setups, and relevant material parameters are given in section 3.1. Then, the simulated frequency response curves of non-plasmonic (section 3.2) and plasmonic (section 3.3) butt-coupled devices are analyzed to study the general impacts of a metal structure on the device performance and its relation to the SBH.

3.1. Simulation methodology

Coupled 3D opto-electrical simulations are performed to obtain performance parameters for both non-plasmonic and plasmonic devices with the following procedure. First, a 3D Finite-Difference-Time-Domain (FDTD) simulation is carried out using Sentaurus Electromagnetic Wave (EMW) Solver [9] to obtain the optical generation profile in the p-i-n region. To mimic the light coming from the Si waveguide in the optical simulation, a monochromatic plane-wave excitation with targeted wavelength of 1.3 μm and optical power intensity of 100W/cm^2 is

placed at the end of the waveguide. The device is surrounded by air (2-μm thick region), and convolutional perfectly matched layer (CPML) type absorbing boundary condition is utilized. The dispersive property of the metal is approached by a single-dipole model provided in Sentaurus EMW Solver. The resulting optical generation profile serves as input in the subsequent electrical transport simulation using Sentaurus Device [9], where a two-step calculation is needed to extract the device performance parameters. First, a quasi-stationary transport simulation based on the drift-diffusion formalisms is performed ramping the bias up to -2 V. Then, a small-signal optical AC analysis is applied to compute the frequency response curve. This curve depicts the QE as function of optical intensity modulation frequency, from which the 3dB bandwidth can be extracted. In the optical AC analysis, a small harmonic perturbation is added to the optical generation as modulation signal. Then, the QE is calculated based on the real part of the perturbation of the current in the device as

$$\eta = \frac{Re(\delta I)/q}{\delta P * \lambda/(hc)},$$ (1)

where δP and δI are the perturbation of optical power absorbed in the p-i-n region and device current, η is the QE and λ is the targeted photon wavelength. The denominator above represents the perturbation of the total number of photons, while the numerator yields the resultant perturbation of the total number of electrons collected by the electrode. The ratio thus gives the internal QE of the photodetector, which does not include the coupling loss from waveguide to p-i-n region. To give an impression for this type of loss, we calculated the coupling efficiency as the ratio of photons incident in the diode region to its total amount from the excitation source at the end of Si WG. These values are about 93% and 68% for the non-plasmonic and plasmonic device, respectively. Additionally, the optical capacitance of the device can be extracted from the optical AC analysis based on the imaginary part of the perturbed device current as follows:

$$C_{\text{opt}} = \frac{1}{\omega} * \frac{Im(\delta I)/q}{\delta P * \lambda/(hc)},$$ (2)

where ω is the modulation frequency and the other symbols represent the same quantities as in Eq. (1). Due to the junction capacitance of the depletion region in the photodetector diode this value is usually positive. A negative C_{opt} would mean that the device becomes abnormally inductive under modulation, leading to an effective RCL or RL small-signal circuit of the device that has band or high-pass response feature, depending on the specific value of the inductance. Thus, plotting C_{opt} as function of the modulation frequency helps to understand the simulated frequency response and to explore unexpected features not typical for a RC-limited curve shape. This will be employed in Section 3.3 for the butt-coupled plasmonic device with moderate SBHs to explain the unusual band-pass feature in the response curves.

In the electrical simulations of the plasmonic devices the metal is included, and its interface with the i-region is modeled as Schottky type. The following set of boundary conditions is applied at this interface:

$$\phi = \phi_{\text{F}} - \phi_{\text{B}} + \frac{k_{\text{B}}T}{q} \ln \left(\frac{N_{\text{c}}}{n_{\text{i,eff}}} \right),$$ (3)

$$j_{\text{n}} \bullet \vec{e}_{\text{n}} = q v_{\text{n}}(n - n_0), \quad n_0 = N_{\text{c}} \exp \left(\frac{-q\phi_{\text{B}}}{k_{\text{B}}T} \right),$$ (4)

$$j_{\text{p}} \bullet \vec{e}_{n} = q v_p(p - p_0), \quad p_0 = N_{\text{v}} \exp \left(\frac{-E_{\text{g}} + q\phi_{\text{B}}}{k_{\text{B}}T} \right).$$ (5)

In the above three equations, ϕ_{F} is the Fermi potential in the metal and ϕ_{B} is the SBH, which is defined as the difference between metal work function (WF) and electron affinity of the (n-type)

semiconductor. The density $n_{i,eff}$ is the effective intrinsic density and $N_{c(v)}$ is the effective density of states for electrons (holes). Default values in Sentaurus Device for the material $In_{0.53}Ga_{0.47}As$ of the i-region are taken for these parameters: 8.404×10^{11} cm^{-3} for $n_{i,eff}$ and 2.54×10^{17} (7.51×10^{18}) cm^{-3} for $N_{c(v)}$. The vector $\vec{e}_n$ is the unit normal vector at the Schottky interface, and $n_0(p_0)$ represents the equilibrium electron (hole) density in the i-region. The thermionic emission velocity for electron (hole) $v_{n(p)}$ is set to the default value of 2.573×10^6 (1.93×10^6) cm/s in Sentaurus Device. Measured values of the WF of Ag vary from 4.52 eV to 4.74 eV depending on the crystal faces [10], and the electron affinity of $In_{0.53}Ga_{0.47}As$ is reported to be 4.5 eV [11]. Considering possible uncertainties of these values and further variations related to other effects like Fermi level pinning [12] [13] and image force [14], we chose to take a wide range of barrier heights, from 0.1 eV to 0.6 eV with a step size of 0.1 eV, to investigate its impact on the device performance. Practically, tuning the barrier height is achieved in the simulations by using a fixed electron affinity (4.5 eV) for the i-region while changing the WF of the metal.

Other important settings for the electrical simulation are described in the following. First, as the Si waveguide is part of the real device, it is also included in the transport simulation by simply attaching it to the i-region as a floating zone (no bias applied). Following Anderson's rule [15], the band offset of the type-II Si/$In_{0.53}Ga_{0.47}As$ hetero-interface is set to 0.46 eV for ΔE_c and to 0.09 eV for ΔE_v. The Si region is undoped, but the i-region is assumed slightly n-doped (1×10^{16} cm^{-3}) as known for III-V materials. The p/n-regions are heavily doped with a concentration of 3×10^{19} cm^{-3}. Traps at material interfaces are disregarded in order to better isolate the impact of the plasmonic structure on the electrostatic behavior. Electron and hole mobilities in Si are set to 1417 cm^2/Vs and 450 cm^2/Vs, respectively, which are the default values in *Sentaurus Device*. In case of $In_{0.53}Ga_{0.47}As$, the values 1100 cm^2/Vs for electrons and 80 cm^2/Vs for holes are used, according to measurements by IBM-Research Zurich. For Shockley-Read-Hall (SRH) lifetimes, the default values in *Sentaurus Device* (10 μs for electrons and 3 μs for holes) are applied to Si, while for $In_{0.53}Ga_{0.47}As$ both are set to 1 ns [16].

3.2. Non-plasmonic butt-coupled WGPD

The study of non-plasmonic device is necessary to identify the limiting carrier transport mechanisms in absence of metal, which helps to further understand plasmonic structure induced device performance changes later. As shown in Fig. 2(a), the frequency response curve of the non-plasmonic device exhibits an unusual "triple cut-off" behavior, with the lowest, intermediate, and highest cut-off frequency at around 30 MHz, 40 GHz and 1 THz, respectively. This indicates that three different transport processes with characteristic times in the μs, ns, and ps range are dominant in determining its response speed, where the one related to the lowest cut-off gives the ultimate limitation to 3dB bandwidth. A similar "double cut-off" feature has been studied in traditional p-n junction Si photodetectors. In these devices, the lower cut-off frequency in the MHz range originates from diffusion of generated carriers outside the high-field depletion region, whereas the higher one at some GHz is related to the transit time or junction capacitance [17]. However, given the small size of the studied device, its junction capacitance is in the order of 10 aF, corresponding to a RC-limited cut-off frequency above 10 PHz, assuming a standard 50 Ω load resistance and no additional parasitic capacitance. Therefore, the junction capacitance is irrelevant for the observed three cut-off frequencies. They should thus be caused by either a drift or diffusion process of electrons or holes in the Si waveguide or in the $In_{0.53}Ga_{0.47}As$ p-i-n region. The standard textbook method used to estimate the origin of the cut-off frequency usually assumes a uniform electric field [17], which is not the case here. The complex geometry of the coupled structure induces a strongly inhomogeneous distribution of both the electric field and the optical generation rate [see Figs. 2(b) and 2(c)].

Here, we introduce a simple and fast method to distinguish between different physical mechanisms related to multiple cut-off frequencies, namely by performing reference studies.
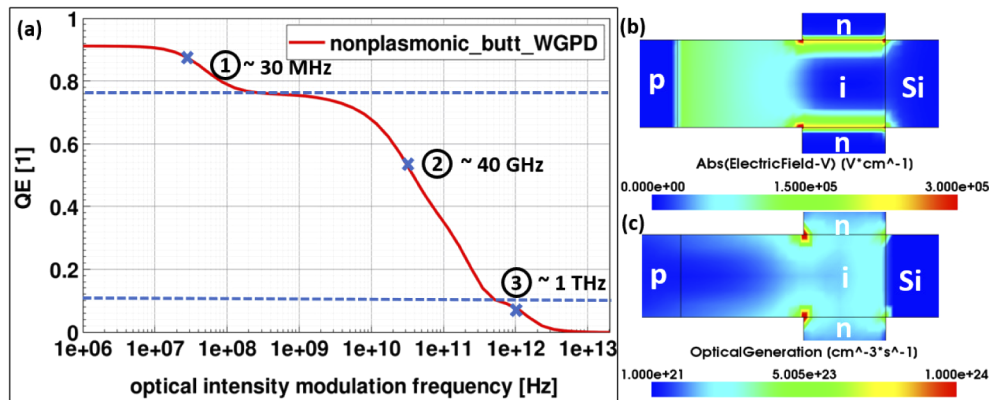
Fig. 2. (a) Frequency response curve of a non-plasmonic butt-coupled WGPD with "triple cut-off" feature. Distribution of (b) electric field and (c) optical generation rate at -2 V, obtained by a horizontal cut at 120 nm below the top surface of the i-region. Color bar from blue to red for electric field (optical generation rate) ranges from 0 to 3×10^5 V/cm (1×10^{21} to 2×10^{24} cm^{-3}s^{-1}).

The method consists in simulating the frequency response of the same structure, but with artificially scaled mobility of one carrier type in one specific region. This is done for all possible combinations of carrier types and device regions. In principle, when the carrier mobility in a high-field region is scaled up, a cut-off frequency should increase if it is limited by the transit time of this type of carrier, since the drift velocity is proportional to the carrier mobility. On the other side, the increase or disappearance of a cut-off after strong decrease of the carrier mobility in a low-field region indicates that diffusion of this carrier type is the limiting mechanism, because the diffusion coefficient is proportional to the mobility (Einstein relation). Furthermore, if the curve shape remains the same after scaling the mobility, then the transport of that carrier type in the studied region should be irrelevant to bandwidth limitation. Based on this logic, transport mechanisms responsible for different cut-offs can be sorted out by comparing the response curves obtained from simulations using different carrier mobilities with the original one. The detailed physics can be understood afterwards by analyzing transport-related quantities in the corresponding region, such as carrier density distribution for diffusion and electric field profile for drift process.

   With this methodology, we found that the curve shape only changes if either scaling down the hole mobility in Si or scaling up the electron and hole mobility in the i-region, with the results shown in Fig. 3(a). The lowest cut-off frequency in the MHz range [labeled as "1" in Fig. 3(a)] increases when the hole diffusion in Si is suppressed or the hole drift in the i-region is speeded up, which means that the lowest cut-off is determined by these transport processes. Furthermore, from the blue (magenta) dashed curve, it is obvious that the intermediate (highest) cut-off frequency should be related to the transit time of holes (electrons) in the i-region, as it scales up with roughly the same factor as the mobility. While the carrier transit time is a well-understood bandwidth-limiting factor in photodetectors [17], the discovered origin of the lowest cut-off frequency due to both hole diffusion from the Si waveguide and hole drift in the i-region is rather abnormal in such a III-V p-i-n structure. Therefore, we focus on understanding the physics behind this observation in the following. Obviously, the occurrence of the diffusion process indicates the existence of a hole density gradient at the Si-waveguide/i-region interface [see Fig. 3(b)]. As shown in Figs. 3(c) and 3(d), this gradient originates from the low drift field and the valence band offset near this interface which leads to a small potential well for holes. The local hole density becomes, therefore, larger than its intrinsic value of 1×10^{10} cm^{-3} in Si.

Consequently, holes from the Si waveguide can only flow into the i-region by diffusion, and holes in the low-field i-region drift with a very small velocity, till they reach the high-field i-region that takes them to the electrode. These slow processes result in the lowest cut-off. This can be further proved by the disappearance of the lowest cut-off frequency when using a slightly n-doped $(1 \times 10^{16} \, \text{cm}^{-3})$ Si waveguide to remove the hole gradient [see red dashed curve in Fig. 3(a)].
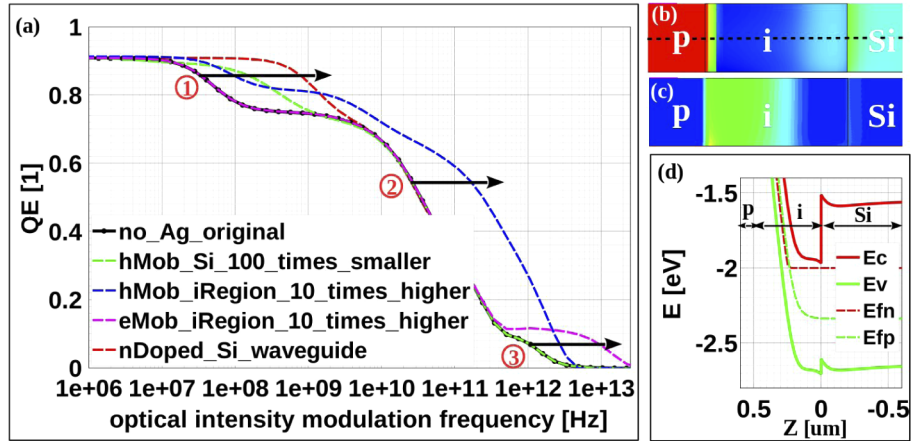
Fig. 3. (a) Frequency response curve of a non-plasmonic butt-coupled WGPD compared with curves obtained using artificially scaled carrier mobilities in Si and i-region, or assuming slightly n-doped $(1 \times 10^{16} \, \text{cm}^{-3})$ Si waveguide. (b) Hole density and (c) electric field profile at -2 V, obtained by a vertical cut in p-i-Si direction along the central line of the i-region. Color bar from blue to red ranges from 3×10^{11} to 3×10 cm^{-3} in (b) and from 0 to 2×10^5 V/cm in (c). (d) Band diagram at -2 V plotted along p-i-Si in z direction, as shown by the black dashed cut-line in (b).

3.3. Plasmonic butt-coupled WGPD

In principle, a metal strip placed on top of the i-region affects the performance of the photodetector by changing both the optics and the electrostatics. From the optics point of view, the presence of a metal alerts the optical mode pattern and thus the optical generation, which impacts the device performance via the amount of optically generated carriers and their distribution. On the other hand, the introduced metal/semiconductor Schottky interface modifies the electric field in the i-region and further changes the performance by influencing the carrier collection there. The interplay of both effects decides its overall impact on the performance, but it could also happen that one of them dominates depending on the device structure and detailed physics. In our case, the impact of the plasmonic structure on the electrostatics is more profound, as will be discussed in the following.

As for the impact on optics, the original dielectric mode in the i-region is hybridized with the plasmonic mode formed at the i-region/Ag interface after placement of the metal [see Figs. 4(a) and 4(b)]. This coupling shifts the mode confinement closer to the interface. As a result, the optical generation rate profile gets more concentrated there, while its volumetric integral over the entire p-i-n region is slightly improved ($4.812 \times 10^9 \, \text{s}^{-1}$ vs. $4.824 \times 10^9 \, \text{s}^{-1}$ in the non-plasmonic vs. plasmonic device). Obviously, its overall influence on the optically generated carriers is relatively small, both in terms of the total amount and the spatial distribution. Therefore, if this were the only impact of the plasmonic structure, the change of the device performance would be negligible. However, adding metal also changes the electric field distribution in the i-region due to the formation of a Schottky barrier that modifies the original band bending in this region.

Naturally, the scope of this modification is related to the SBH, and the effect should already exist once a metal strip is present, i.e. even in the dark, unbiased device. Lighting and biasing just amplify the effect while maintaining the same pattern. This is shown in Fig. 4(c), where the electric field distributions in non-plasmonic and plasmonic butt-coupled devices are compared for all studied SBHs in dark and unbiased condition, along with the illuminated device at a reverse bias of -2 V and a SBH of 0.6 eV as example.It can be seen that according to the change of the electric field along the p-i-Si direction in the i-region covered by Ag, the metal-induced electrostatic effects can be grouped into two types depending on the SBH. For barriers lower than 0.4 eV, the field becomes more intense in the part of the i-region close to the p/i junction, whereas for high barriers (0.4 eV to 0.6 eV) the field enhancement happens in a region far from it. The reason is the different band bending at different positions in the i-region along the p-i-Si direction, which varies with the SBH. For example, at a point far from the p/i junction, the band bends up for all values of the SBH as expected for an n-type Schottky barrier (note that the i-region is slightly n-doped). The bending becomes weaker with decreasing SBH [see Fig. 4(d) obtained at a distance of 450 nm from the p/i junction]. This explains the observed stronger field enhancement close to the i/Si interface for higher barriers. When moving towards the p/i junction, the degree of this up-bending decreases for all barrier heights [for example, at 250 nm from the p-region shown in Fig. 4(e)]. Eventually, the band bends down when getting very close to the p/i junction, except for very high barriers [see Fig. 4(f) obtained at 50 nm from the p/i junction]. This down-bending becomes more pronounced for smaller barrier heights, in accordance with the stronger field near the p/i junction for low barriers. The trend change in band bending along the p-i-Si direction actually originates from the presence of the p/i junction that causes a change of the energetic position of the Fermi level in the i-region. As can be seen from the band diagram along the p-i-Si direction of the original non-plasmonic device shown in Fig. 4(g), the energetic distance between valence band edge and Fermi level decreases towards the p/i junction with the consequence that also the energetic distance between the Fermi levels of metal and i-region changes. The latter determines the shape of the Schottky barrier, i.e. the band bending.

To illustrate this behavior, we take a barrier height of 0.1 eV at positions far from and close to the p/i junction as examples. Far from the p/i junction [with a distance of 450 nm, marked by the blue dashed line in Fig. 4(g)], the Fermi level in the i-region (blue-colored dashed line, labeled E_{fn1}) is close to the conduction band edge, and the energetic distance between them [0.06 eV as shown in Fig. 4(h)] is smaller than the barrier height of 0.1 eV. Thus, the Fermi level in the i-region lies above the one in the metal and, consequently, the band bends up at this position [see red-colored band edge in Fig. 4(d)]. However, as the semiconductor Fermi level in the i-region moves into the gap when approaching the p/i junction, it will at some point undercut the metal Fermi level, as shown by the orange-colored dashed line, labeled E_{fn2} at 50 nm distance to the p/i junction, which leads to a down-bending of the bands [see red-colored band in Fig. 4(f)]. Obviously, the smaller the SBH, the earlier this transition happens when moving towards the p-region and the stronger the down-bending at a given position close to the p/i junction. The change of the band bending direction is related to the change of the field direction in the corresponding regions, which strongly alters the carrier flow and eventually causes abnormal response curves in case of low barriers as will be shown below. In summary, the placement of metal significantly changes the properties of the electric field in the metal-covered i-region, including its intensity distribution pattern and pointing direction, depending on the SBHs. Therefore, the change of the electrostatics caused by the plasmonic structure should have a large influence on the device performance, because the speed of the carrier collection process mainly depends on the field.

Figure 5 shows the frequency response curves of the plasmonic butt-coupled WGPD with all SBHs, in comparison to the non-plasmonic one.It turns out that placing a plasmonic structure mostly impacts its response around the original lowest cut-off frequency in the reference device
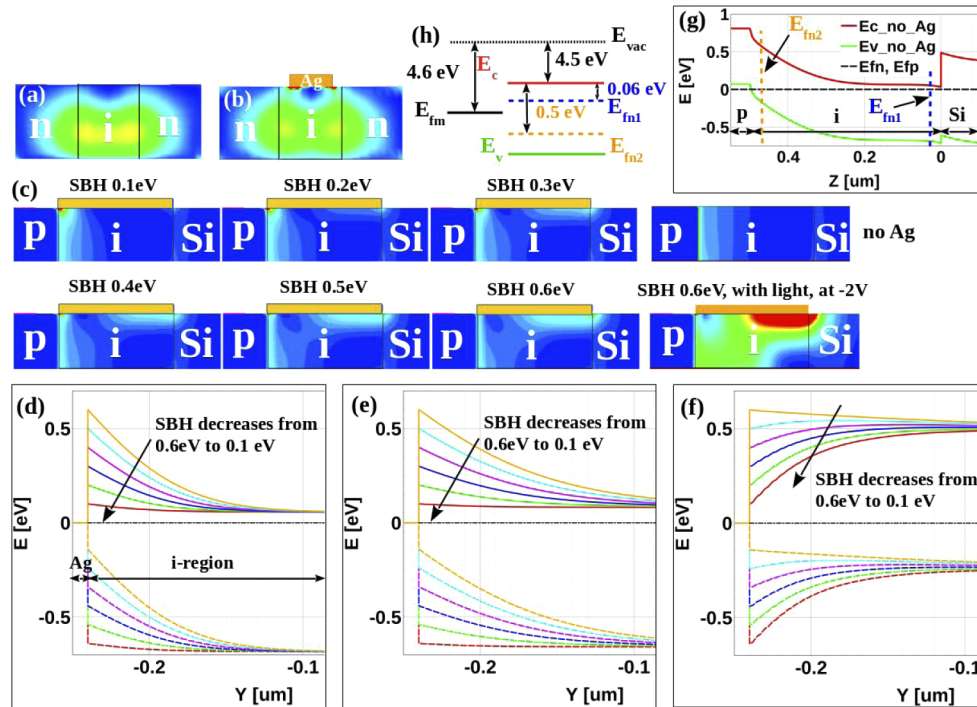
Fig. 4. (a)/(b) Optical generation rate profile of non-plasmonic/plasmonic butt-coupled WGPDs, obtained by a vertical cut along the n-i-n direction at 100 nm distance from the i/Si interface. Color bar from blue to red changes from 3×10^{21} to 3×10^{23} cm^{-3}s^{-1}. (c) Electric field profiles in the dark at 0 V for non-plasmonic and plasmonic butt-coupled WGPDs with varied barrier heights, together with the profile under light at -2 V for a SBH of 0.6 eV. Color bar from blue to red ranges from 0 to 3×10^{5} V/cm. (d)/(e)/(f) Band diagrams at the Schottky interface for plasmonic devices with varied barrier heights in the dark at 0 V, obtained by a vertical cut along y direction at positions with a distance of 450nm/250nm/50nm from the p/i junction. Colored solid (dashed) and black dashed lines represent CB (VB) edge and Fermi level in the i-region, respectively. (g) Band diagram along p-i-Si (z direction) of the non-plasmonic butt-coupled WGPD in the dark at 0 V obtained by a horizontal cut at 120 nm below the top surface of the i-region. The blue and orange dashed lines mark the positions with a distance of 450 nm and 50 nm from the p/i junction, respectively, showing that the Fermi level approaches the valence band edge (from E_{fn1} to E_{fn2}) when moving towards the p-region. (h) Detailed flat-vacuum band alignment at the Ag/i-region interface in case of a SBH of 0.1 eV, corresponding to a distance of 50 nm (orange dashed line) and 450 nm (blue dashed line) from the p/i junction labeled in (g).

without metal (see label "1" in Fig. 5), which can be either improved with SBHs higher than 0.4 eV or degraded with lower ones. Furthermore, the change of the curve shape related to this lowest cut-off differs between low (below 0.4 eV) and high (above 0.3 eV) barriers. High barriers mainly change the original second QE plateau that occurs in the range from 0.1 GHz to 10 GHz in the non-plasmonic case. The lowest cut-off frequency decreases as the barrier becomes lower. The DC QE is not affected so that the shape remains similar as in the non-plasmonic device. On the other hand, the curve shape changes notably for barriers lower than 0.4 eV. The typical shape of a RC-time limited response curve disappears, instead a band-pass feature shows up in the MHz to GHz frequency range, leading to a significant drop of the DC QE. According to the reference studies for the lowest cut-off in the non-plasmonic case shown in Fig. 3(a), a change of the second QE plateau can only be related to hole drift in the i-region, but not to hole diffusion from Si, and neither of them can alter the DC QE. Therefore, the following hypothesis of the origins of the observed performance change in this lowest cut-off frequency range can be constructed. First, for barriers higher than 0.3 eV, hole drift in the i-region should still be the main limiting process, while hole diffusion in Si is no more relevant. Secondly, for barriers lower than 0.4 eV, new physical mechanisms must exist, which cause the new band-pass feature and thus the drop of the DC QE. They must be related to the transport at the Schottky interface, since this is the only process additionally introduced to the device by the placement of the metal. To clarify this issue, the reference study method described in Section 3.2 is again employed. Here it is advantageous to use 0.3 eV and 0.4 eV as examples for a relatively low and high barrier, respectively.
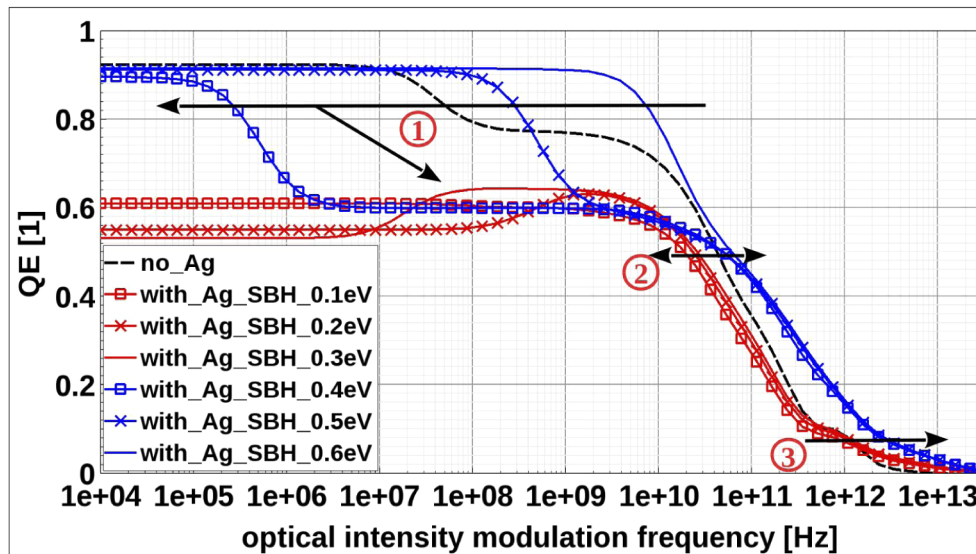
Fig. 5. Comparison of frequency response curves of non-plasmonic and plasmonic butt-coupled WGPDs, with Schottky barrier heights varying from 0.1 eV to 0.6 eV. The lowest, middle, and highest cut-off frequency in the original non-plasmonic device are labeled as "1", "2" and "3", with arrows showing their changes after metal placement.

To explore the case of a high barrier (0.4 eV), the same reference studies using a scaled hole mobility in the i-region and in Si are performed as had been done in the non-plasmonic case. Figure 6(a) shows, that the lowest cut-off frequency indeed scales up with roughly the same factor when increasing the hole mobility in the i-region by a factor of 10 (blue solid curve with square markers), while the curve shape hardly changes when strongly suppressing the hole mobility in Si (green solid curve with circle markers). The elimination of hole diffusion from Si comes from the largely enhanced electric field near the i/Si interface in the case of high barriers [see

color map for field intensity shown in Fig. 6(b)], which had been explained before. It supports the drift of carriers since a hole density gradient no more exists [see Fig. 6(c)]. For the device with a low SBH (0.3 eV), the occurrence of the band-pass feature which is a typical RCL-limited response suggests that the device behaves somehow inductively in the corresponding frequency range. This can be confirmed by calculating its optical capacitance C_{opt} based on Eq. (2).In Fig. 6(d) the spectral C_{opt}-curves of non-plasmonic and plasmonic devices with low (0.3 eV) and high (0.4 eV) barrier are compared. As can be seen, C_{opt} is positive when an RC-limited response is obtained (in case of non-plasmonic and plasmonic butt-coupled WGPDs with high barrier). It only becomes negative in the MHz range when the band-pass feature occurs in the device with small SBH. The band-pass resonance frequency is related to the detailed values in the equivalent RCL circuit, which is out of the scope of this work. Here we focus on the qualitative understanding of the physical mechanisms that lead to the reversion of the optical impedance. According to studies reported in [18] and [19], an inductive behavior has been observed in highly forward-biased Schottky diodes, which is most likely caused by the conductivity modulation induced by the large amount of injected minority carriers. In our devices, though such an injection is not directly present as the metal is not biased, a similar flow of minority carriers actually exists in the i-region. It is carried by holes in the i-region near the p/i junction flowing from the metal interface into the i-region (see arrows labeling the hole current flow in Fig. 6(e) for a low barrier of 0.3 eV). This hole current originates from the strong down-bending of the bands there, which happens for low barriers as explained before, and which makes the electric field pointing from the metal into the i-region. On the other hand, due to the up-bending bands in the i-region far from the p/i junction, holes in this part are flowing towards the metal interface. This leads to a hole current flow flipping in a large part of the i-region beneath the metal, i.e. to a kind of rotating current which behaves effectively like an inductor and results in a negative optical capacitance C_{opt}. To confirm this hypothesis, we run another reference simulation by reducing the thermionic emission velocity of holes at the Schottky interface. By doing so, the contribution of the "circular" minority current should be largely reduced, and eventually the band-pass feature should disappear. This indeed happens as can be seen from the red solid curve with square markers in Fig. 6(a). Furthermore, although an opposite hole current flow also exists in some regions of the device with a SBH of 0.4 eV [see arrows for hole current flow in Fig. 6(b)], the inductive effect does not show up there. The reason is that the down-bending of bands occurs later in the case of higher barriers when moving towards the p/i junction, as explained before, which leads to a smaller amount of minority carrier injection that is simply not sufficient to totally reverse the behavior from a capacitive into an inductive one. Nevertheless, the change of the current flow caused by the Schottky interface formation induces an additional limit to the device response. This can be seen from the observed increase of the lowest cut-off frequency when scaling up the thermionic emission velocity of holes by a factor of 10 [blue solid curve with cross markers in Fig. 6(a)] .

In order to further examine the robustness of the observed metal-induced performance changes with respect to the applied reverse bias, we simulate the device response under -1 V, -2 V and -3 V for all studied SBHs. Results for the cases of 0.3 eV (low) and 0.4 eV (high) SBH are shown in Fig. 7(a) as examples. As can be seen, the shape of the response curve for a given SBH basically remains the same under changed bias, though the cut-off frequencies are slightly affected with detailed impacts depending on the relevant limiting mechanisms.The middle and highest cut-off [labeled as "2" and "3" in Fig. 7(a)] that are determined by drift of holes and electrons in the i-region, increase with higher reverse bias for both low and high SBHs. This is simply because of the corresponding higher electric field at stronger reverse bias, as shown in Fig. 7(b). The new lowest cut-off [labeled "1" in Fig. 7(a)] which is related to the change of hole current flow induced by the Schottky interface, decreases as the reverse bias increases for both low and high SBHs, although the origin is slightly different. For a high SBH of 0.4 eV, increasing the reverse
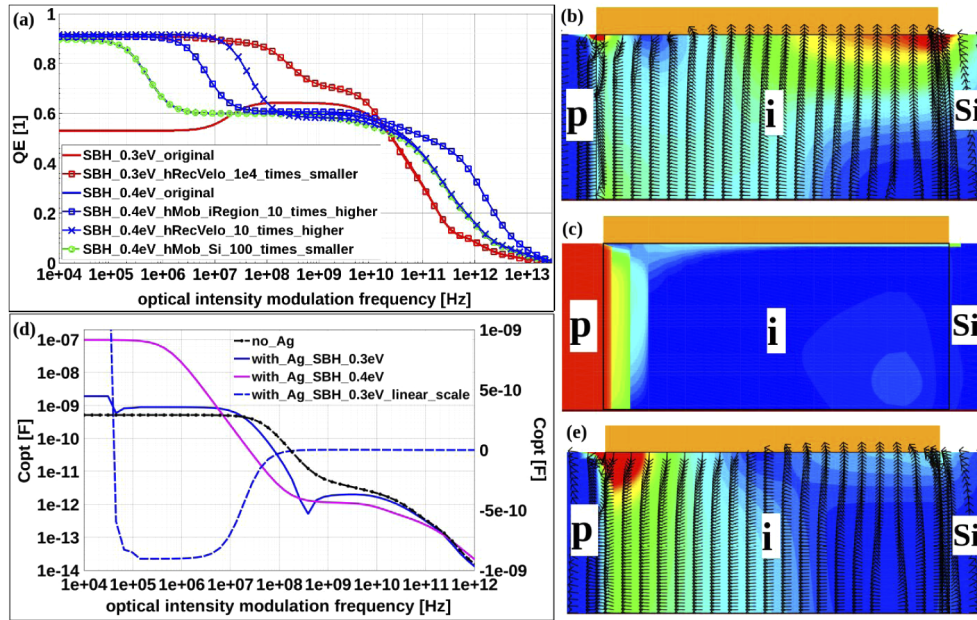
Fig. 6. (a) Frequency response curves of plasmonic butt-coupled WGPDs with barrier heights of 0.4 eV and 0.3 eV, respectively, together with curves obtained from reference studies. (b) Electric field and (c) hole density profile at -2 V of a plasmonic device with barrier height of 0.4 eV, obtained by a vertical cut in the p-i-Si direction along the central line of the i-region. Color bar from blue to red ranges from 0 to 3×10^5 V/cm in (b) and from 3×10^{11} to 3×10^{19} cm^{-3} in (c). (d) Comparison of spectral optical capacitance C_{opt} of non-plasmonic and plasmonic butt-coupled devices with barrier heights of 0.4 eV and 0.3 eV, respectively. The left y-axis is in log-scale, where the dips in the case of a 0.3 eV barrier (blue solid line) are due to the sign change of C_{opt}. The latter becomes obvious in the linear-scale plot on the right y-axis (blue dashed line). (e) Electric field profile at -2 V in the plasmonic device with a SBH of 0.3 eV, obtained by a vertical cut in p-i-Si direction along the central line of the i-region. Color bar from blue to red ranges from 0 to 3×10^5 V/cm. Arrows in (b) and (e) indicate the direction of the hole current flow.

bias leads to a stronger band bending, thus a higher hole current flow from metal in the i-region near the p/i junction, as seen from the color-map of the hole current density in Figs. 7(c) and 7(d). Consequently, the lowest cut-off becomes more determined by this metal-induced current component and, thus, decreases as bias increases. This phenomenon had already been observed when we studied the dependency of the response change on SBH, where the lowest cut-off frequency drops when lowering the barrier within the high SBH range due to the stronger flipping of the hole current flow, as shown in Fig. 5 by the orange/cyan/magenta-colored curves for a SBH decreasing from 0.6 eV to 0.4 eV. For the low SBH case (0.3 eV), a higher reverse bias causes an earlier flipping of the hole current direction, i.e. the hole current flow from the metal appears in a larger part of the i-region [see Figs. 7(e) and 7(f)], which indicates a more inductive behavior, and, thus a lower RCL resonance frequency, resulting in a reduced lowest cut-off. An extended current flow from the metal also means that more carriers get collected instead of flowing into the metal far from the p/i junction, resulting in a higher DC QE as can be inferred from the blue-colored curves in the low-frequency range.
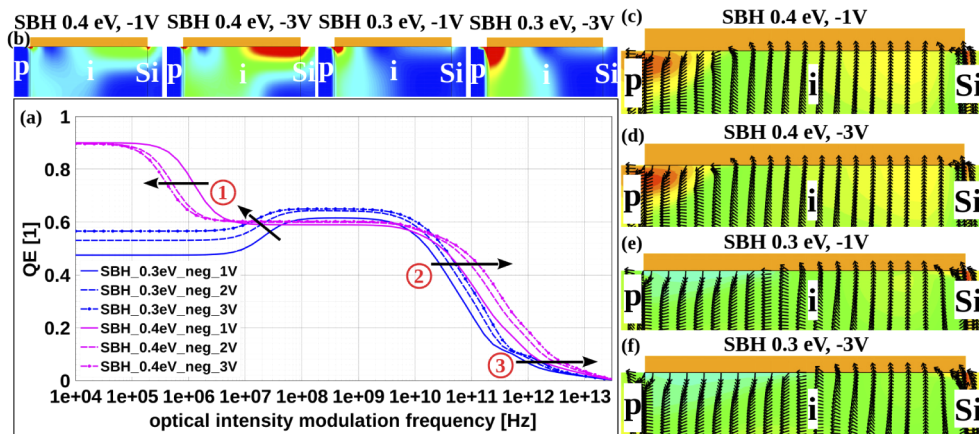
Fig. 7. (a) Frequency response curves of plasmonic butt-coupled WGPDs with barrier heights of 0.4 eV and 0.3 eV under bias of -1 V, -2 V and -3 V. (b) Electric field at -1 V and -3 V of a plasmonic device with barrier height of 0.4 eV and 0.3 eV, obtained by a vertical cut in the p-i-Si direction along the central line of the i-region. Color bar from blue to red ranges from 0 to 3×10^5 V/cm. (c) and (d) / (e) and (f) Hole current density profile at -1 V and -3 V in the plasmonic device with a SBH of 0.4 eV/0.3 eV, obtained by a vertical cut in p-i-Si direction along the central line of the i-region. Color bar from green to red ranges from 0.1 to 10 A/cm^2. Arrows indicate the direction of the hole current flow.

4. Conclusion

In this work, we theoretically investigated how a plasmonic structure placed on the i-region impacts the performance of a butt-coupled p-i-n type WGPD in terms of its frequency response. In particular, the metal-induced electrostatic impacts and the dependence on the Schottky barrier height are emphasized, which is rarely discussed in researches related to this field. It is found that for the plasmonic device with relatively high barriers above 0.3 eV, the 3dB bandwidth decreases as the barrier becomes lower. As long as the barrier is higher than 0.4 eV, its cut-off frequency outperforms the non-plasmonic device. In the case of barriers lower than 0.4 eV an abnormal band-pass feature resulting in a strong drop of the DC QE is found in the MHz range of the response curves. It most likely originates from the large amount of opposite hole current flow in the i-region benenath the metal. All these effects are related to the band bending in the metal-covered i-region, which depends on its position and the barrier height. The spatial dependence is caused by the varying energetic distance between Fermi level and band edges in the i-region due to the presence of the p/i junction. Additionally, the observed metal-induced impacts on the device response are rather insensitive with respect to a change of the reverse bias in the reasonable range from -1 V to -3 V. Based on above conclusions, we suggest that in the future design of plasmonic photodetectors, the impacts of the metal structure on the electrostatics as well as the choice of the material pair that determines the Schottky barrier height should be taken into account carefully in order to avoid an undesired deterioration of the device performance.

Disclosures. The authors declare no conflicts of interest.

Data availability. Data underlying the results presented in this paper are not publicly available at this time but may be obtained from the authors upon reasonable request.

References

1. A. Hirata and M. Yaita, "Ultrafast terahertz wireless communications technologies," IEEE Trans. Terahertz Sci. Technol. **5**, 1128–1132 (2015).
2. A. Dorodnyy, Y. Salamin, P. Ma, J. Vukajlovic Plestina, N. Lassaline, D. Mikulik, P. Romero-Gomez, A. Fontcuberta i Morral, and J. Leuthold, "Plasmonic Photodetectors," IEEE J. Sel. Top. Quantum Electron. **24**(6), 1–13 (2018).
3. Y. Salamin, P. Ma, B. Baeuerle, A. Emboras, Y. Fedoryshyn, W. Heni, B. Cheng, A. Josten, and J. Leuthold, "100 GHz Plasmonic Photodetector," ACS Photonics **5**(8), 3291–3297 (2018).
4. J. Gosciniak, F. B. Atar, B. Corbett, and M. Rasras, "Plasmonic Schottky photodetector with metal stripe embedded into semiconductor and with a CMOS-compatible titanium nitride," Sci. Rep. **9**(1), 6048 (2019).
5. J. Gosciniak and M. Rasras, "High-bandwidth and high-responsivity waveguide-integrated plasmonic germanium photodetector," J. Opt. Soc. Am. B **36**(9), 2481–2491 (2019).
6. Q. Ding, S. Sant, and A. Schenk, "Design Strategy for Monolithically Integrated Photodetector and Improvement using Plasmonics," in *2019 International Conference on Numerical Simulation of Optoelectronic Devices (NUSOD)* (2019), pp. 155–156.
7. H. Schmid, M. Borg, K. Moselund, L. Gignac, C. M. Breslin, J. Bruley, D. Cutaia, and H. Riel, "Template-assisted selective epitaxy of III-V nanoscale devices for co-planar heterogeneous integration with Si," Appl. Phys. Lett. **106**(23), 233101 (2015).
8. S. Mauthe, Y. Baumgartner, M. Sousa, Q. Ding, M. D. Rossell, A. Schenk, L. Czornomaz, and K. E. Moselund, "High-speed iii-v nanowire photodetector monolithically integrated on si," Nat. Commun. **11**(1), 4565 (2020).
9. Synposys, "Sentaurus Device & Electromagnetic Wave (EMW) Solver," (2018). Version-O-2018.06.
10. A. W. Dweydari and C. H. B. Mee, "Work function measurements on (100) and (110) surfaces of silver," Physica Status Solidi (A) **27**(1), 223–230 (1975).
11. P. E. Smith, S. H. Goss, M. Gao, M. K. Hudait, Y. Lin, S. A. Ringel, and L. J. Brillson, "Atomic diffusion and band lineups at $In_{0}.53Ga_{0}.47As$-on-InP heterointerfaces," J. Vac. Sci. Technol., B: Microelectron. Process. Phenom. **23**(4), 1832–1837 (2005).
12. A. M. Cowley and S. M. Sze, "Surface states and barrier height of metal-semiconductor systems," J. Appl. Phys. **36**(10), 3212–3220 (1965).
13. W. Mönch, "Chemical trends of barrier heights in metal-semiconductor contacts: on the theory of the slope parameter," Appl. Surf. Sci. **92**, 367–371 (1996).
14. A. Tugulea and D. Dascălu, "The image-force effect at a metal-semiconductor contact with an interfacial insulator layer," J. Appl. Phys. **56**(10), 2823–2831 (1984).
15. R. L. Anderson, "Germanium-Gallium Arsenide Heterojunctions [Letter to the Editor]," IBM J. Res. Dev. **4**(3), 283–287 (1960).
16. R. K. Ahrenkiel, R. Ellingson, S. Johnston, and M. Wanlass, "Recombination lifetime of $In_{0}.53Ga_{0}.47As$ as a function of doping density," Appl. Phys. Lett. **72**(26), 3470–3472 (1998).
17. G. Ghione, Semiconductor devices for high-speed optoelectronics (Cambridge University Press, 2009).
18. T. Misawa, "Impedance of bulk semiconductor in junction diode," J. Phys. Soc. Jpn. **12**(8), 882–890 (1957).
19. J. Werner, A. F. J. Levi, R. T. Tung, M. Anzlowar, and M. Pinto, "Origin of the excess capacitance at intimate schottky contacts," Phys. Rev. Lett. **60**(1), 53–56 (1988).